High precision isotope micro-imaging of materials

Hisayoshi Yurimoto[*], Kazuhide Nagashima, Takuya Kunihiro

Department of Earth and Planetary Sciences, Tokyo Institute of Technology, Meguro, Tokyo 152-8551, Japan

Abstract

Secondary ion mass spectrometry (SIMS) is widely used to identify the isotope ratio of the micro-area of materials. We demonstrate that the precision and spatial resolution of an ion microscope using SIMS coupled with a newly developed solid-state ion imager can be extended to two-dimensional isotope ratio imaging with permil-precision. An isotopic map for oxygen clearly reveals the distribution of 4% enrichment of ^{16}O in spinel particles embedded in melilite from a Ca–Al-rich inclusion of a carbonaceous chondrite. This characterization technique called *isotopography* thus provides the eyes to see small heterogeneity of isotope abundance in micro-scale. It is likely to find broad application in earth, material, and life science research.
© 2002 Elsevier Science B.V. All rights reserved.

Keywords: SIMS; Imaging; Isotope; Ion detector; Oxygen; Meteorite

1. Introduction

Analysis of isotope and trace element distribution in heterogeneous micro-structures has become increasingly crucial for diagnosing natural and biological materials and for predicting the properties of synthetic devices. Imaging by secondary ion mass spectrometry (SIMS) has been applied for the purpose but this has been generally limited to trace element mapping as it has not been possible to obtain quantitative measurements from the image.

Stigmatic and scanning methods have been proposed for imaging by SIMS [1]. Both methods achieve micron to sub-micron image resolution but the error in isotope analysis was limited to >5% [2] because of the difficulty of accumulating sufficient secondary ions. This difficulty is mainly due to nonideal properties of the detection system such as narrow dynamic range, large dead time, nonlinear output and high noise. Since these properties introduce errors for imaging greater than natural isotopic variation, the application of SIMS imaging was limited to samples having large isotopic heterogeneity such as pre-solar grains [2] or else to element analysis of biological tissue [3]. Here we demonstrate high precision isotope micro-imaging by means of SIMS with a solid-state ion imager. For this purpose, a perfectly suited specimen exhibiting heterogeneous isotope composition among constituent materials within micro-area has been selected.

The specimen is found in a Ca–Al-rich inclusion (CAI), HN3-1, from a carbonaceous chondrite, Allende CV3 [4]. A high mass-resolution stigmatic SIMS instrument (Cameca IMS 1270) that provides a mass-filtered stigmatic secondary ion image of the sample surface with a high spatial resolution [5] and a high-efficiency stacked CMOS-type active pixel sensor (SCAPS) [6] was used for the experiment. The SCAPS has several advantages over conventional detection systems including two-dimensional detection,

[*] Corresponding author. Tel.: +81-3-5734-2336;
fax: +81-3-5734-3538.
E-mail address: yuri@geo.titech.ac.jp (H. Yurimoto).

wide dynamic range, no insensitive period, direct detection of charged particles, and constant ion-detection sensitivities among nuclides [7]. Hence, SCAPS can measure high ion flux with an accuracy of within twice the statistical error and with a detection limit corresponding to 10 incident ions [8].

2. Experimental

CAIs, micro-scale mineral aggregates which are a component of chondritic meteorites, are the oldest material generated in the solar system [9]. It is well known that O isotopes are distributed heterogeneously
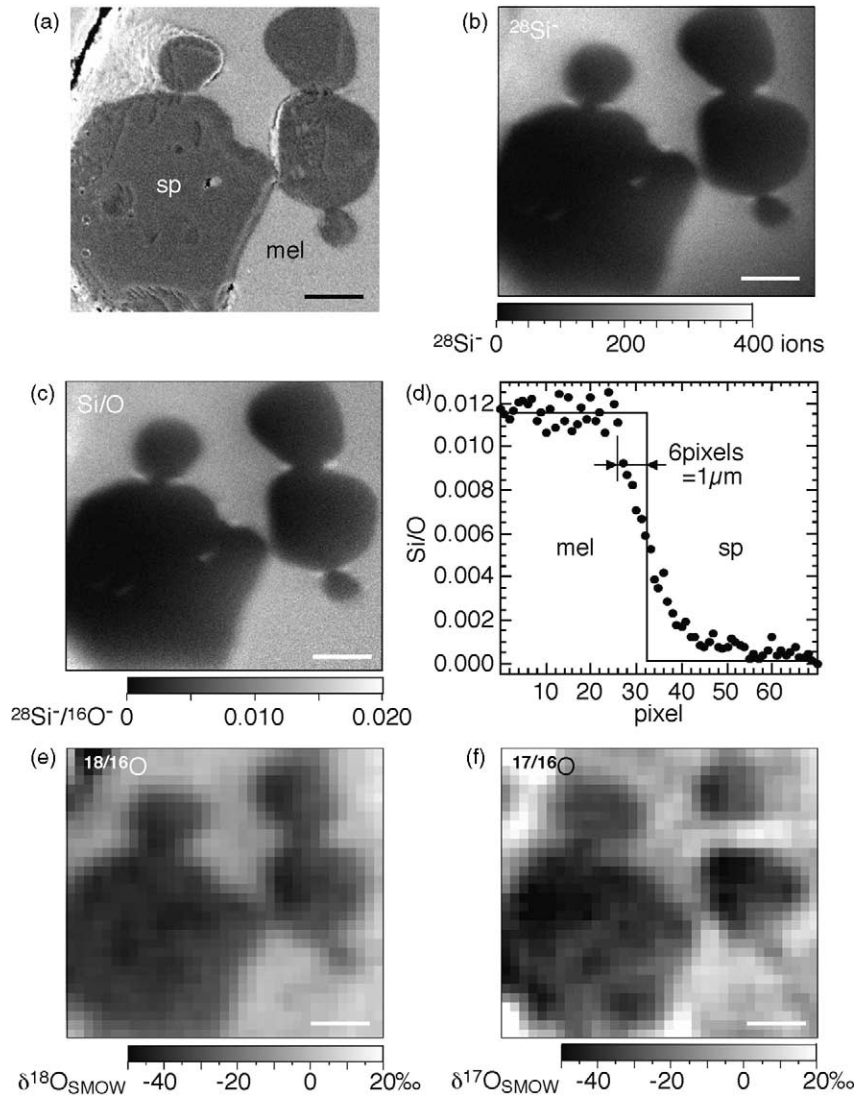

Fig. 1. Analyzed area of a CAI, HN3-1. Back-scattered image (a), secondary ion image (b) for $^{28}Si^-$, and secondary ion ratio image (c) for $^{28}Si^-/^{16}O^-$. Small spinal grains (sp) are enclosed in a melilite single crystal (mel). Cross section (d) of $^{28}Si^-/^{16}O^-$ between melilite and spinel. An ideal variation between the phases is also illustrated. Isotope ratio images, *isotopography*, for $^{18}O/^{16}O$ (e) and $^{17}O/^{16}O$ (f). Since Cs^+ primary beam sputtered the sample surface about 3 μm depth during accumulation of (e) and (f) images. Outlines of spinel grains slightly differ between both the images. A crack existing in the upper left corner provides artifact distribution in the O isotope ratio images. Scale bars: 10 μm.

among the constituent minerals. Such a material is ideal for demonstrating precise isotope imaging, because the variation of O isotope ratios among the minerals is <5%. A polished thin section with a gold coating (30 nm depth) of a CAI named HN3-1, categorized as coarse-grained type B1, from the Allende CV3 meteorite was prepared for this study. Spinel and melilite are major minerals in HN3-1 and spinel grains are poikilitically enclosed in large melilite single crystal (Fig. 1a).

The oxygen isotope abundance found in nature is typically $(^{16}O,^{17}O,^{18}O) = (99.763, 0.0372, 0.1995)$, and the relative variation in nature is normally less than a few percent. In order to describe the O isotope ratio with such a small variation, we use δ-value

$$\delta^{17\,\text{or}\,18}O_{\text{SMOW}} \equiv \left\{ \frac{(^{17\,\text{or}\,18}O/^{16}O)_{\text{sample}}}{(^{17\,\text{or}\,18}O/^{16}O)_{\text{SMOW}}} - 1 \right\} \times 1000‰$$

where SMOW means standard mean ocean water. The O isotope ratios ($\delta^{17}O_{\text{SMOW}}, \delta^{18}O_{\text{SMOW}}$) for the spinel and melilite in HN3-1 were (−42.8, −40.5) and (−4.3, −0.5), respectively [10]. The homogeneous O isotope distributions within both mineral phases have been established by spot analysis using SIMS [11,12].

Oxygen isotope imaging has been performed on the area in Fig. 1a. The area was homogeneously irradiated by a Cs^+ primary ion beam (20 keV, 45 nA) by rastering (80 μm × 80 μm). A normal incident electron gun was used for charge compensation of the area.

When we analyze O isotope ratios by SIMS, molecular interferences become a problem [13]. The most serious interference is from $^{16}OH^-$ for the $^{17}O^-$ peak. In order to separate the $^{16}OH^-$ contribution from the $^{17}O^-$ peak, the mass spectrometer of IMS 1270 was adjusted to high mass-resolution mode with a power $(M/\Delta M) > 4700$. Mass spectra were taken by SCAPS at around 17 amu before every imaging analysis in order to confirm that enough mass-resolution was obtained. The mass dispersion plane of IMS 1270 was directly projected onto SCAPS. Fig. 2 shows that the intensity of $^{16}OH^-$ peak is about 8% relative to that of the $^{17}O^-$ peak. Furthermore, the $^{16}OH^-$ peak is clearly separated from the $^{17}O^-$ peak. The small $^{16}OH^-$ peak was cut by the mass selection slit of IMS 1270. Under this condition, interference-free imaging for all O isotopes was collected by SCAPS.
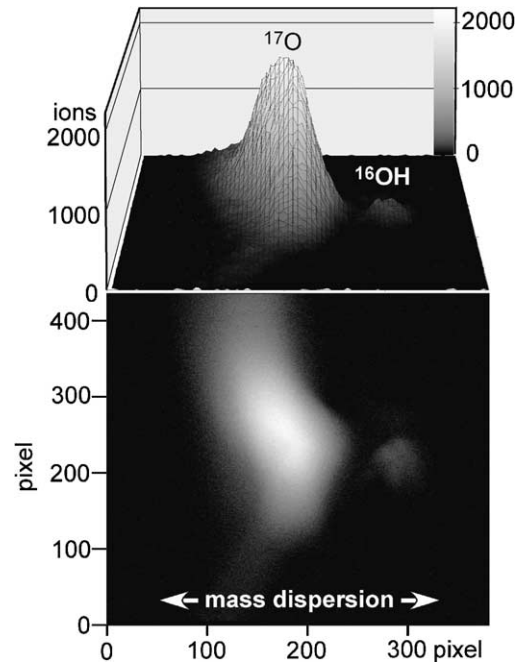

Fig. 2. A typical mass spectrum at 17 amu region, acquired in 400 s. The $^{17}O^-$ peak profile (∼2100 ions at the top) is clearly separated from $^{16}OH^-$ peak profile (∼170 ions at the top).

Secondary ions generated by the primary beam were used to construct a mass-filtered ion image using stigmatic ion optics of IMS 1270 and directly projected onto the 315 × 288 pixel matrix of SCAPS (Fig. 1b–f). One pixel in Fig. 1b and c corresponds to 0.17 μm × 0.17 μm on the sample surface.

In order to accumulate sufficient signals in SCAPS, secondary ion images were acquired for $^{28}Si^-$, $^{16}O^-$, $^{17}O^-$ and $^{18}O^-$ in this order with integration times of 38, 19, 1103 and 735 s, respectively. The average number of ions per pixel accumulated for $^{28}Si^-$, $^{16}O^-$, $^{17}O^-$ and $^{18}O^-$ images was estimated to be 240, 17 000, 400 and 1200, respectively.

3. Results and discussion

The $^{28}Si^-$ image (Fig. 1b) clearly shows a distribution of spinel and melilite corresponding to that shown in Fig. 1a, but the secondary ion emission from melilite is not homogeneous. This is probably due to a small difference in electrostatic energy state on

the sample surface because of incomplete charge compensation. However, if we use the secondary ion ratio instead of secondary ion intensity for imaging, e.g., a $^{28}Si^-/^{16}O^-$ image, this analytical artifact is corrected (Fig. 1c). The spatial resolution of the image, defined by the width for the signal to drop to one-half, is six pixels between signals for spinel and melilite (Fig. 1d). This width corresponds to 1 μm on the sample.

The statistical error (1σ) or shot noise in images constructed from ions accumulated in a pixel was estimated to be ∼50 and ∼30‰ for the $^{17}O^-/^{16}O^-$ and $^{18}O^-/^{16}O^-$ images, respectively. Although the error for $^{18}O/^{16}O$ is slightly smaller than the difference in δ-value deference between spinel and melilite, the error for $^{17}O/^{16}O$ is larger. Thus, in order to reduce the statistical error, successive digital image processing using pixel binning with a 9×9 pixel matrix and using a moving-average through neighboring pixels was applied to simple secondary ion ratio images of $^{17}O^-/^{16}O^-$ and $^{18}O^-/^{16}O^-$.

The O isotope ratio images after image processing are shown in Fig. 1e and f. Since we obtained the $^{16}O^-$, $^{17}O^-$ and $^{18}O^-$ images successively, the secondary ion ratio values were not directly equivalent to the isotope ratios because variation of secondary ion intensities through analysis cannot be ignored. The ion ratio images also include instrumental mass fractionation of SIMS. Therefore, in order to correct the offset components, we normalized the average $^{17}O^-/^{16}O^-$ and $^{18}O^-/^{16}O^-$ ratios for spinel to the δ-value for $^{17}O/^{16}O$ and $^{18}O/^{16}O$ obtained by conventional methods [10], respectively. The O isotope ratio images of Fig. 1e and f clearly demonstrate that ^{16}O-component is enriched in spinel compared to melilite. The spatial resolution of the images, however, was reduced to 2 μm from 1 μm in the original image due to the image processing.

The precision of the O isotopic analysis is quantitatively evaluated using O isotopic distribution in the spinel and melilite grains (Fig. 3). The standard deviation in $\delta^{18}O$ for spinel and melilite corresponds to 2.7 and 4.2‰, respectively, while that for $\delta^{17}O$ is 5.4 and 6.3‰, respectively, for the two phases. Statistical standard deviation after image processing is estimated to be 3‰ for $\delta^{18}O$ and 6‰ for $\delta^{17}O$. Therefore, the observed values are consistent with calculated statistical errors.

The histograms clearly show that two independent kinds of O isotope components exist in the CAI. The difference of O isotopic ratio between the two peaks is 40 and 44‰ for $\delta^{17}O$ and $\delta^{18}O$, respectively. The δ-value differences are in good agreement with the results obtained by the conventional method for the mineral
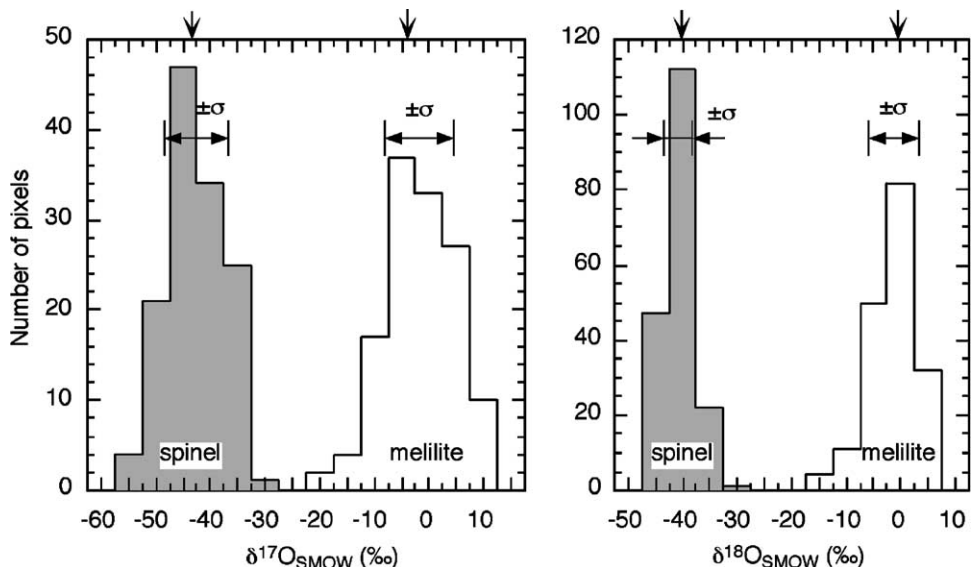

Fig. 3. Histogram of O isotopic composition in spinel and melilite grains. A band indicated by both the side arrows on each distribution (labeled by $\pm\sigma$) shows standard deviation from the average isotope ratio of the phase. Recommended values by conventional method are shown by vertical arrows on upper axes.

separated samples [10]. In conclusion, these results clearly confirm and illustrate the inter- and intra-mineral O isotopic distribution in the CAI estimated by point analyses [11], i.e., O isotope ratios are distributed homogeneously within spinel and in melilite, but those of individual minerals differ from each other, with those changing sharply at the grain boundary.

4. Summary

This study unambiguously demonstrates that high precision isotope ratio imaging of micro-scale under high mass-resolution is possible by the combination of SIMS and SCAPS. Since this technique opens a new research field in the isotope micro-texture of materials, we shall name the field *isotopography*; which also means topography of isotopes. Isotopography will be widely useful as a powerful technique for solving practical problems in all research fields using microscopes and micro-analysis, e.g., not only earth science as in this paper but also material and life sciences. In the state of the art, however, permil-precision with micron-resolution is barely sufficient for recording. More sophisticated ion optics such as multi-imaging optics and more efficient detectors with lower noise would be useful to improve accuracy of isotopography.

References

[1] A. Benninghoven, F.G. Rüdenauer, H.W. Werner, Secondary Ion Mass Spectrometry: Basic Concepts, Instrumental Aspects, Applications and Trends, Wiley, New York, 1987, p. 1227.
[2] P. Hoppe, R. Strebel, P. Eberhard, S. Amari, R.S. Lewis, Meteoritic Planet. Sci. 35 (2000) 1157–1176.
[3] S. Chandra, D.R. Smith, G.H. Morrison, Anal. Chem. 72 (2000) 104A–114A.
[4] H. Nagahara, H. Nagasawa, N. Nakamura, T. Matsui, Lunar Planet. Sci. 18 (1987) 694–695.
[5] E. de Chambost, T. Rouxel, A. Pflieger, M. Schuhmacher, in: A. Benninghoven, Y. Nihei, R. Shimizu, H.W. Werner (Eds.), Secondary Ion Mass Spectrometry (SIMS IX), Wiley, New York, 1994, pp. 274–277.
[6] I. Takayanagi, et al., in: Proceedings of the 1999 IEEE Workshop on Charge-Coupled Devices and Advanced Image Sensors, 1999, pp. 159–162.
[7] K. Nagashima et al., Surf. Interf. Anal. 31 (2001) 131–137.
[8] T. Kunihiro et al., Nucl. Instrum. Meth. Phys. Res. 470 (2001) 512–519.
[9] G.J. MacPherson, D.A. Wark, J.T. Armstrong, in: J.F. Kerridge, M.S. Matthews (Eds.), Meteorites and the Early Solar System, University of Arizona Press, Tucson, AZ, 1988, pp. 746–807.
[10] T.K. Mayeda, N.R. Clatton, H. Nagasawa, Lunar Planet. Sci. 17 (1986) 526–527.
[11] H. Yurimoto, H. Nagasawa, Y. Mori, O. Matsubaya, Earth Planet. Sci. Lett. 128 (1994) 47–53.
[12] M. Ito, H. Yurimoto, H. Nagasawa, Lunar Planet. Sci. 29 (1998) 1556.
[13] H. Yurimoto, M. Ito, H. Nagasawa, Science 282 (1998) 1874–1877.